IMMUNOLOGY

# NDR2 promotes the antiviral immune response via facilitating TRIM25-mediated RIG-I activation in macrophages

**Zhiyong Liu[1], Cheng Wu[1], Yueyun Pan[1], Huan Liu[1], Xiumei Wang[1], Yuting Yang[1], Meidi Gu[1], Yuanyuan Zhang[2], Xiaojian Wang[1]***



**Retinoic acid–inducible gene I (RIG-I), a pivotal cytosolic sensor, recognizes viral RNAs to initiate antiviral innate immunity. However, posttranslational regulation of RIG-I signaling is not well understood. We report here that nuclear Dbf2-related kinase 2 (NDR2) functions as a crucial positive regulator of the RIG-I–mediated antiviral immune response. Overexpression of NDR2 or its kinase-inactive mutants potentiates RNA virus–induced production of type I interferons and proinflammatory cytokines and dampens viral replication. NDR2 conditional knockout mice (Lysm$^{+}$NDR2$^{f/f}$) show an impaired antiviral immune response. Mechanistically, NDR2 directly associates with RIG-I and TRIM25, thus facilitating the RIG-I/TRIM25 complex and enhancing the TRIM25-mediated K63-linked polyubiquitination of RIG-I, which is required for the RIG-I–mediated antiviral immune response. Furthermore, NDR2 expression is notably down-regulated in peripheral blood from respiratory syncytial virus–infected patients and in virus-infected macrophages. Collectively, these findings provide insights into the function of NDR2 in antiviral immunity and its related clinical significance.**

## INTRODUCTION

The innate immune system functions as the frontier of host defense to sense and fight against microbial pathogen invasion via recognition of pathogen-associated molecular patterns aided by pattern recognition receptors (PRRs) (*1*). Among these PRRs, retinoic acid–inducible gene I (RIG-I)–like receptors (RLRs) serve as cytoplasmic RNA sensors that recognize viral RNA and trigger signaling cascades that induce antiviral mediators, such as type I interferons (IFNs) and proinflammatory cytokines (*2*). RIG-I, the most important RLR, recognizes a wide variety of RNA viruses, including influenza A virus (IAV), Sendai virus (SeV), respiratory syncytial virus (RSV), and vesicular stomatitis virus (VSV) (*2*). Following ligand binding, RIG-I is activated from a "closed" conformation to an "open" conformation and is recruited to the mitochondria-associated membrane where it binds to the scaffold protein MAVS (mitochondrial antiviral signaling protein) and promotes a massive aggregation of MAVS. Then, recruited kinases, such as transforming growth factor β–activated kinase 1 (TAK1) and TANK binding kinase 1 (TBK1), are phosphorylated, which leads to the activation of nuclear factor κB (NF-κB), mitogen-activated protein kinase (MAPK), and IFN regulatory factor (IRF) pathways (*3*). Subsequently, type I IFNs are induced by the cooperation of activated IRF3 and NF-κB. Then, IFNs trigger the Janus kinase (JAK)/signal transducers and activators of transcription (STAT) signaling pathway to increase the expression of IFN-stimulated genes (ISGs), which function as vital effectors in the intracellular antiviral defense program and adaptive immunity modulation (*4*).

Posttranslational modification of RIG-I by different types of ubiquitination is a key event in the modulation of RIG-I–triggered NF-κB, MAPK, and IRF activation. The E3 ligases tripartite motif–containing protein 25 (TRIM25) (*5*), Riplet (*6*), TRIM4 (*7*), and MEX3C (Mex-3 RNA binding family member C) (*8*) have been shown to conjugate covalent K63-linked polyubiquitin chains to RIG-I to mediate its activation. Alternatively, RIG-I also undergoes K48-linked ubiquitination by RNF125 (ring finger protein 125) (*9*) and c-Cbl (casitas B-lineage lymphoma proto-oncogene) (*10*) for proteasomal degradation to form a negative feedback loop of RIG-I signaling. Considering the importance of RIG-I ubiquitination in an RIG-I–mediated antiviral immune response, the assembly of these ubiquitin chains for RIG-I must be tightly regulated. Liu *et al.* (*11*) recently demonstrated that cyclophilin A enhances the interaction between RIG-I and TRIM25 during SeV infection, which resulted in increased TRIM25-mediated K63-linked ubiquitination of RIG-I and facilitated recruitment of RIG-I to MAVS.

NDR2 [nuclear Dbf2 (dumbbell forming protein 2)–related kinase 2], also known as STK38L (serine/threonine-protein kinase 38-like) , is a member of the serine/threonine kinases and belongs to the NDR/LATS (large tumor suppressor) subfamily (including NDR1, NDR2, LATS1, and LATS2), which is highly conserved in eukaryotes (*12*). NDR2 has been implicated in a variety of biological processes ranging from cell division to apoptosis and tumorigenesis (*13*). NDR2 can also act as a proapoptotic kinase in a fatty acid synthase receptor–induced apoptosis pathway via the formation of an MST1 (mammalian STE20-like protein kinase 1)–NDR–MOB1 (Mps one binder 1) complex downstream of Ras association domain-containing protein 1 (RASSF1A) (*14*). Devroe *et al.* (*15*) reported that NDR2 kinase is cleaved by HIV-1 protease (PR), which alters NDR2 subcellular localization and inhibits the enzymatic activity of NDR2. However, the role of NDR2 in an antiviral innate immune response has not been established.

Here, we report that NDR2 deficiency selectively restrains RIG-I–sensing RNA virus infection–induced type I IFNs and proinflammatory cytokine expression. Consistently, Lysm$^{+}$NDR2$^{f/f}$ mice, in which NDR2 is conditionally deleted in the myelomonocytic and osteoclast lineages, are more sensitive to RNA virus VSV and IAV (H1N1 subtype) infection than wild-type (WT) control mice. We further identify that NDR2 directly interacts with RIG-I and TRIM25 and promotes the K63-linked polyubiquitination of RIG-I mediated by TRIM25, leading to enhanced RIG-I pathway activation and downstream

[1]Institute of Immunology, School of Medicine, Zhejiang University, Hangzhou 310058, Zhejiang, China. [2]The Children's Hospital, School of Medicine, Zhejiang University, Hangzhou 310058, China.
*Corresponding author. Email: wangxiaojian@cad.zju.edu.cn

expression of type I IFNs. Furthermore, NDR2 expression is significantly attenuated in peripheral blood mononuclear cells (PBMCs) from RSV-infected patients and virus-infected macrophages.

## RESULTS

### NDR2 selectively promotes an anti-RNA virus immune response in a kinase activity–independent manner

We recently demonstrated that NDR1 promotes an antiviral innate immune response by binding to the intergenic region of miR146a to repress miR146a transcription, which leads to the potentiated translation of STAT1 (*16*). NDR1 and NDR2 have >80% amino acid identity and play similar roles in various biological processes (*12*). Cornils *et al.* (*17*) demonstrated that the abundance of the NDR2 protein was increased upon knockout of NDR1 in a tissue-specific manner. However, there was no significant difference of NDR2 expression in WT and NDR1 knockout peritoneal macrophages (PMs) (fig. S1A). To evaluate the function of NDR2 in an antiviral innate immune response, we tested the expression of NDR2 in various murine primary immune cells and the thymus. NDR2 was ubiquitously expressed, with the highest levels observed in PMs (fig. S1B). Thus, we generated NDR2 conditional knockout mice that specifically target deletion in the myelomonocytic and osteoclast lineages by crossing $NDR2^{f/f}$ mice with Lysm-Cre transgenic mice. PMs (fig. S1C) and bone marrow–derived macrophages (BMDMs) (fig. S1D) from $Lysm^{+}NDR2^{f/f}$ mice had decreased expression of NDR2 but had similar expression of NDR1 compared to those from $NDR2^{f/f}$ mice. Together, these data indicate that there is no compensation between NDR1 and NDR2 expression in macrophages.

We next sought to determine the effect of NDR2 on viral infection–induced type I IFNs and proinflammatory cytokine production in the murine primary macrophages obtained from $NDR2^{f/f}$ and $Lysm^{+}NDR2^{f/f}$ mice. As shown in Fig. 1, A and B, and fig. S1E, NDR2 knockout markedly restrained the protein and mRNA levels of IFN-β, IL-6 (interleukin-6), and TNF-α (tumor necrosis factor–α) in PMs (Fig. 1, A and B) and BMDMs (fig. S1E) upon VSV infection. Correspondingly, virus infection–induced IFN-β, IL-6, and TNF-α expression was inhibited in NDR2 knockdown PMs (fig. S1, F and G) and human PBMCs (fig. S1H). Low–molecular weight (LMW) polyinosinic:polycytidylic acid [poly(I:C)] [a melanoma differentiation-associated protein 5 (MDA5) agonist] intracellular transfection, which activates the RIG-I pathway, triggered less IFN-β, IL-6, and TNF-α mRNA expression in NDR2-deficient PMs (fig. S1I). We further investigated the contribution of NDR2 to the antiviral innate immune response by infecting PMs with other types of viruses. As shown in Fig. 1C, upon infection with H1N1, SeV, and RSV (sensed by RIG-I), but not with encephalomyocarditis virus (EMCV, an RNA virus sensed by MDA5) or DNA virus [herpes simplex virus–1 (HSV-1) and murine gammaherpesvirus 68 (MHV68), sensed by cyclic adenosine 5′-monophosphate–guanosine 3′,5′-monophosphate synthase (cGAS)], NDR2-deficient PMs expressed lower IFN-β, IL-6, and TNF-α mRNA than WT PMs, indicating that NDR2 selectively promotes RIG-I–sensing RNA virus–induced type I IFNs and proinflammatory cytokine expression in PMs. In addition, NDR2 has no effect on intracellular high–molecular weight (HMW) poly(I:C) (an MDA5 agonist)–induced IFN-β and proinflammatory cytokine expression in PMs (fig. S1J). We performed fluorescence-activated cell sorting (FACS) analysis and a 50% tissue culture infective dose ($TCID_{50}$) assay to further investigate the impact of NDR2 on virus replication. NDR2 deficiency facilitated VSV replication in PMs (Fig. 1, D and E) while this deficiency did not affect HSV-1 replication (fig. S1K), indicating that NDR2 selectively suppresses RNA virus infection.

As a protein kinase, NDR2 reportedly phosphorylates different substrates to influence a variety of biological processes, including ciliogenesis, neurite formation, and cell survival (*18*–*20*). To investigate whether NDR2 inhibited RNA virus infection via its kinase activity, we constructed two NDR2 kinase–inactive mutant-expressing plasmids [K119M and K282A/T442A (AA)] (*21*) and transfected NDR2-deficient PMs with these plasmids. As shown in Fig. 1F, NDR2-deficient PMs showed an impaired production of IFN-β, IL-6, and TNF-α induced by VSV, which was rescued to levels comparable to WT PMs upon reexpression of Flag-tagged NDR2 or its kinase-inactive mutants. Correspondingly, we observed lower virus replication (Fig. 1G and fig. S1L) and higher expression of IFN-β, IL-6, and TNF-α (fig. S1M) in the stably Flag-tagged NDR2 or its kinase-inactive mutants overexpressed in RAW264.7 macrophages compared to control transfectants after VSV infection. Together, these data suggest that NDR2 positively regulates the host innate immune response against RNA virus in a kinase activity–independent manner. An immunoblot assay confirmed the efficiency of NDR2 knockdown (fig. S1N) and overexpression in macrophages (fig. S1, O and P).

### NDR2 is critical for protecting mice from RNA virus infection

We next determined NDR2-mediated antiviral responses in vivo. In a mouse model of VSV infection with a moderate dose, $Lysm^{+}NDR2^{f/f}$ mice expressed lower levels of type I IFNs and proinflammatory cytokines in serum (Fig. 2A), PMs (fig. S2A), and the spleen (fig. S2B) compared to $NDR2^{f/f}$ mice. The elevated viral burden was observed in spleens, lungs, and livers of $Lysm^{+}NDR2^{f/f}$ mice (Fig. 2B and fig. S2C). Meanwhile, pathological analysis revealed that VSV infection resulted in increased alveolar hemorrhaging, alveolar wall thickening, and severe edema in the lungs of $Lysm^{+}NDR2^{f/f}$ mice compared with WT mice (Fig. 2C). Meanwhile, the number of neutrophils ($CD11b^{+}Gr\text{-}1^{+}$) was quantified by FACS analysis in bronchoalveolar lavage fluid (BALF) from VSV-infected $NDR2^{f/f}$ and $Lysm^{+}NDR2^{f/f}$ mice. As shown in Fig. 2D, $Lysm^{+}NDR2^{f/f}$ mice displayed significantly higher VSV-induced neutrophil recruitment in BALF than $NDR2^{f/f}$ mice. Accordingly, all eight VSV-infected $Lysm^{+}NDR2^{f/f}$ mice died within 48 hours after infection, whereas four of eight (50%) VSV-infected $NDR2^{f/f}$ mice survived and remained healthy for the duration of the overall survival assay (Fig. 2E). We also intranasally infected mice with H1N1 virus and monitored the survival of these mice. We observed more than 90% mortality in $Lysm^{+}NDR2^{f/f}$ mice 15 days after infection, whereas the mortality of WT mice was less than 40% at this time point (Fig. 2F). After H1N1 infection, the viral burden was significantly higher in the lungs of $Lysm^{+}NDR2^{f/f}$ mice than that of $NDR2^{f/f}$ mice (Fig. 2G). Consistent with data from in vitro experiments (Fig. 1C and fig. S1K), there was no significant difference in the overall survival assay (fig. S2D), viral burden in the brain (fig. S2E), or the production of IFN-β, IL-6, and TNF-α in serum (fig. S2F) between $NDR2^{f/f}$ and $Lysm^{+}NDR2^{f/f}$ mice challenged with HSV-1. Collectively, these results indicate that NDR2 effectively protects the host against RNA virus infection with an augmented production of type I IFNs and proinflammatory cytokines in vivo.

### NDR2 promotes virus-triggered signaling at the RIG-I level

We then investigated how NDR2 promotes RIG-I–sensing RNA virus–triggered type I IFNs and proinflammatory cytokine production.

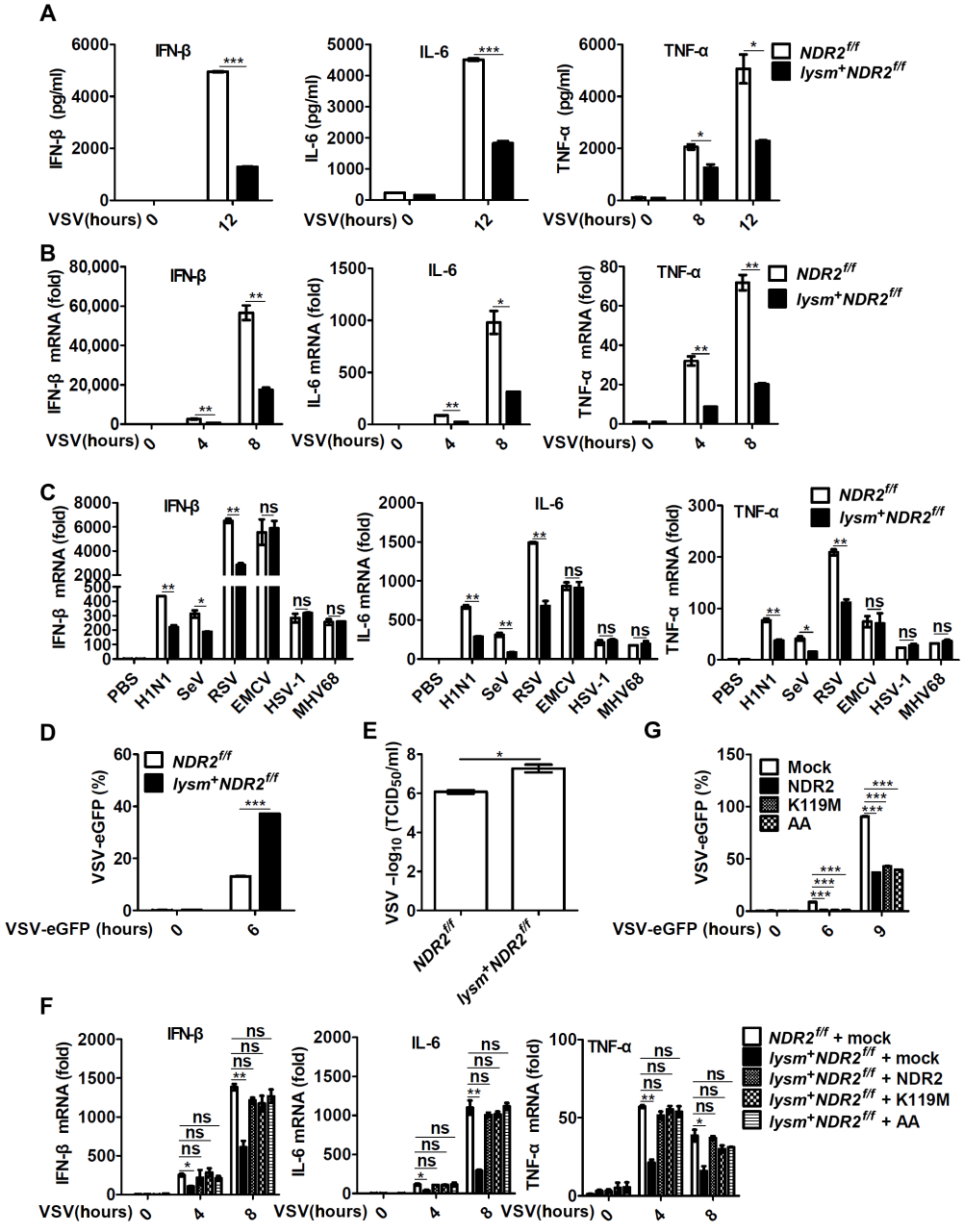


**Fig. 1. NDR2 facilitates RNA virus–induced IFN-β, IL-6, and TNF-α production via a kinase activity–independent mechanism in macrophages.** (**A** and **B**) IFN-β, IL-6, and TNF-α expression in *NDR2*$^{f/f}$ and *Lysm*$^{+}$*NDR2*$^{f/f}$ PMs infected with VSV in the indicated times was detected by enzyme-linked immunosorbent assay (ELISA) (A) and real-time polymerase chain reaction (PCR) analysis (B). (**C**) Real-time PCR analysis of IFN-β, IL-6, and TNF-α transcripts in *NDR2*$^{f/f}$ and *Lysm*$^{+}$*NDR2*$^{f/f}$ PMs treated with phosphate-buffered saline (PBS) or with the infection of H1N1, SeV, RSV, EMCV, HSV-1, or MHV68 for 8 hours. (**D**) Fluorescence-activated cell sorting (FACS) analysis of enhanced green fluorescent protein (eGFP) fluorescence intensity in *NDR2*$^{f/f}$ and *Lysm*$^{+}$*NDR2*$^{f/f}$ PMs infected with VSV-eGFP. (**E**) VSV-eGFP titers by $TCID_{50}$ assay in supernatants of *NDR2*$^{f/f}$ and *Lysm*$^{+}$*NDR2*$^{f/f}$ PMs infected with VSV-eGFP for 6 hours. (**F**) *NDR2*$^{f/f}$ and *Lysm*$^{+}$*NDR2*$^{f/f}$ PMs were transfected with empty vector (mock), NDR2, or its kinase-inactive mutants overexpressing plasmids for 36 hours and then infected with VSV, followed by real-time PCR analysis of IFN-β, IL-6, and TNF-α expression. AA, K282A/T442A. (**G**) FACS analysis of RAW264.7 cells stably overexpressing NDR2 or its kinase-inactive mutants infected with VSV-eGFP. Data are means ± SD and are representative of three independent experiments. Student's *t* test was used for statistical calculation. ns, no significance. $^{*}P < 0.05$, $^{**}P < 0.01$, and $^{***}P < 0.001$.

The phosphorylation of TBK1, IRF3, P65, ERK1/2 (extracellular signal–regulated kinase 1/2), JNK1/2 (c-Jun N-terminal kinase 1/2), and P38 was significantly inhibited in Lysm$^{+}$NDR2$^{f/f}$ PMs relative to NDR2$^{f/f}$ PMs upon VSV (Fig. 3A) or SeV (Fig. 3B) infection. Consistently, knockdown of NDR2 also decreased the phosphorylation of these key proteins in RIG-I signaling in BMDMs with VSV infection (Fig. 3C). Meanwhile, LMW poly(I:C) intracellular transfection triggered much less TBK1, IRF3, P65, ERK1/2, JNK1/2, and P38 phosphorylation in NDR2-deficient PMs (Fig. 3D). NDR2 deficiency does not affect EMCV-induced (fig. S3A), intracellular HMW

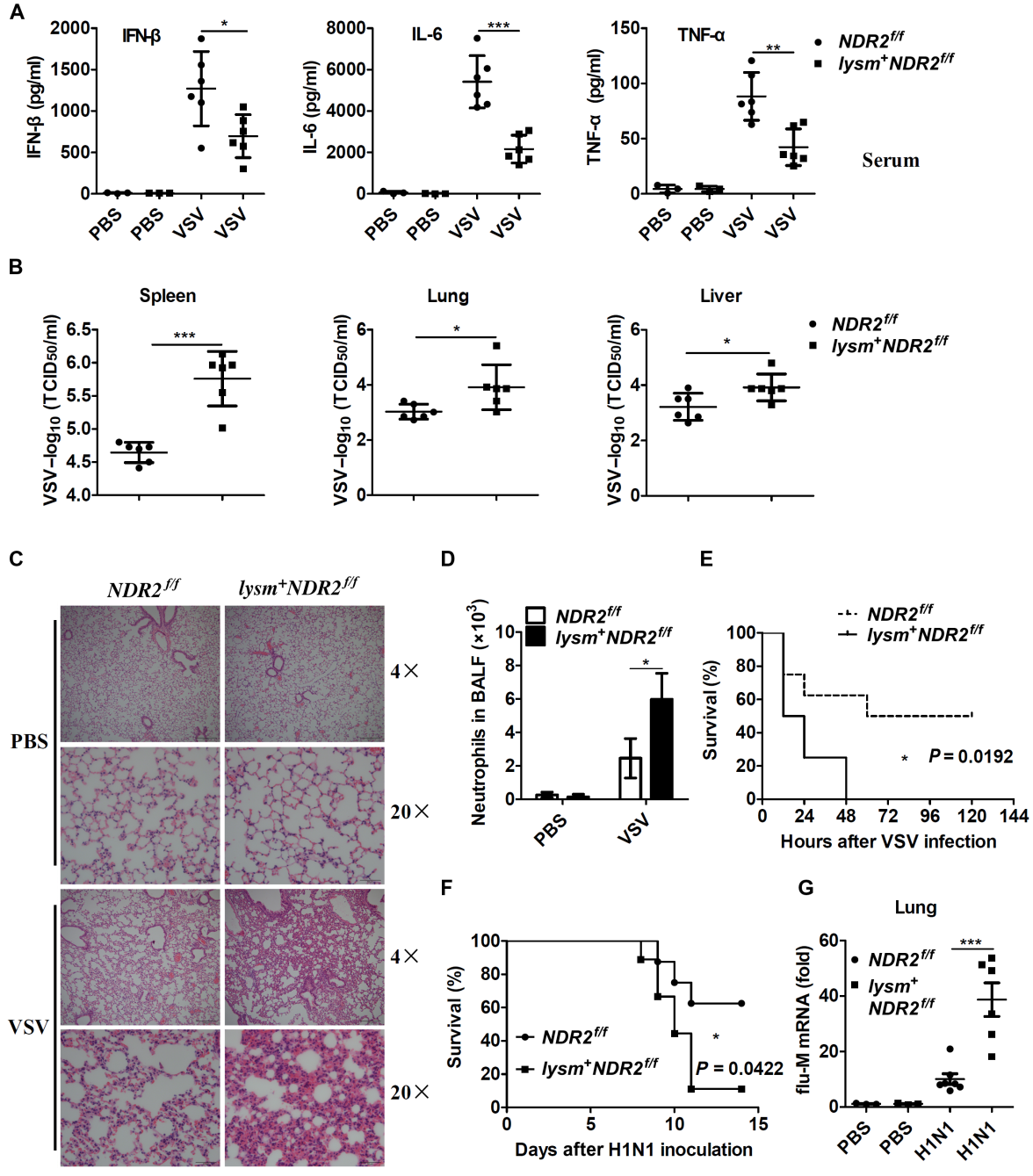


**Fig. 2. *NDR2*-deficient mice are more vulnerable to RNA viral infection.** (**A**) ELISA of IFN-β, IL-6, and TNF-α in serum obtained from 8-week-old male $NDR2^{f/f}$ and $Lysm^{+}NDR2^{f/f}$ mice ($n = 6$ per group) 12 hours after intraperitoneal infection with VSV [$1 \times 10^7$ plaque-forming units (PFU) $g^{-1}$]. (**B**) VSV titers by $TCID_{50}$ assay in spleens, lungs, and livers from mice in (A). (**C**) Pathology of $NDR2^{f/f}$ and $Lysm^{+}NDR2^{f/f}$ mice in response to VSV infection. Hematoxylin and eosin staining of lung sections from mice in (A). Scale bars, 200 μm (for 4×) and 50 μm (for 20×). (**D**) Neutrophil ($CD11b^{+}Gr\text{-}1^{+}$) infiltration in murine bronchoalveolar lavage fluid (BALF) from mice treated with intraperitoneal injections of PBS ($n = 3$) or VSV ($1 \times 107$ PFU $g^{-1}$ and $n = 3$) was assessed 12 hours after injection. (**E**) Survival of 8-week-old male $NDR2^{f/f}$ and $Lysm^{+}NDR2^{f/f}$ mice administered VSV ($1 \times 10^8$ PFU $g^{-1}$) via tail intravenous injection ($n = 8$ per group; Wilcoxon test). (**F**) Survival curve for 8-week-old male $NDR2^{f/f}$ ($n = 8$) and $Lysm^{+}NDR2^{f/f}$ ($n = 9$) mice infected with H1N1 virus ($2 \times 10^3$ PFU per mouse) by intranasal inoculation (Wilcoxon test). (**G**) Real-time PCR analysis of flu-M mRNA of lungs from 8-week-old male $NDR2^{f/f}$ and $Lysm^{+}NDR2^{f/f}$ mice 4 days after intranasal inoculation with H1N1 virus ($2 \times 10^3$ PFU per mouse) ($n = 6$ per group). Data are means ± SD and are representative of three independent experiments. Student's *t* test was used for statistical calculation. $^{*}P < 0.05$, $^{**}P < 0.01$, and $^{***}P < 0.001$.

poly(I:C)–induced (fig. S3B), or HSV-1–induced (fig. S3C) activation of these pathways in PMs. Reexpression of NDR2 or its kinase-inactive mutants in $Lysm^{+}NDR2^{f/f}$ PMs rescued VSV-induced RIG-I signaling activation to a level comparable to that observed in $NDR2^{f/f}$ PMs (Fig. 3E). Overexpression of NDR2 or its kinase-inactive mutants promoted the phosphorylation of TBK1, IRF3, P65, ERK1/2, JNK1/2, and P38 in RAW264.7 macrophages during VSV infection (fig. S3D). Moreover, overexpression of NDR2 or its kinase-inactive

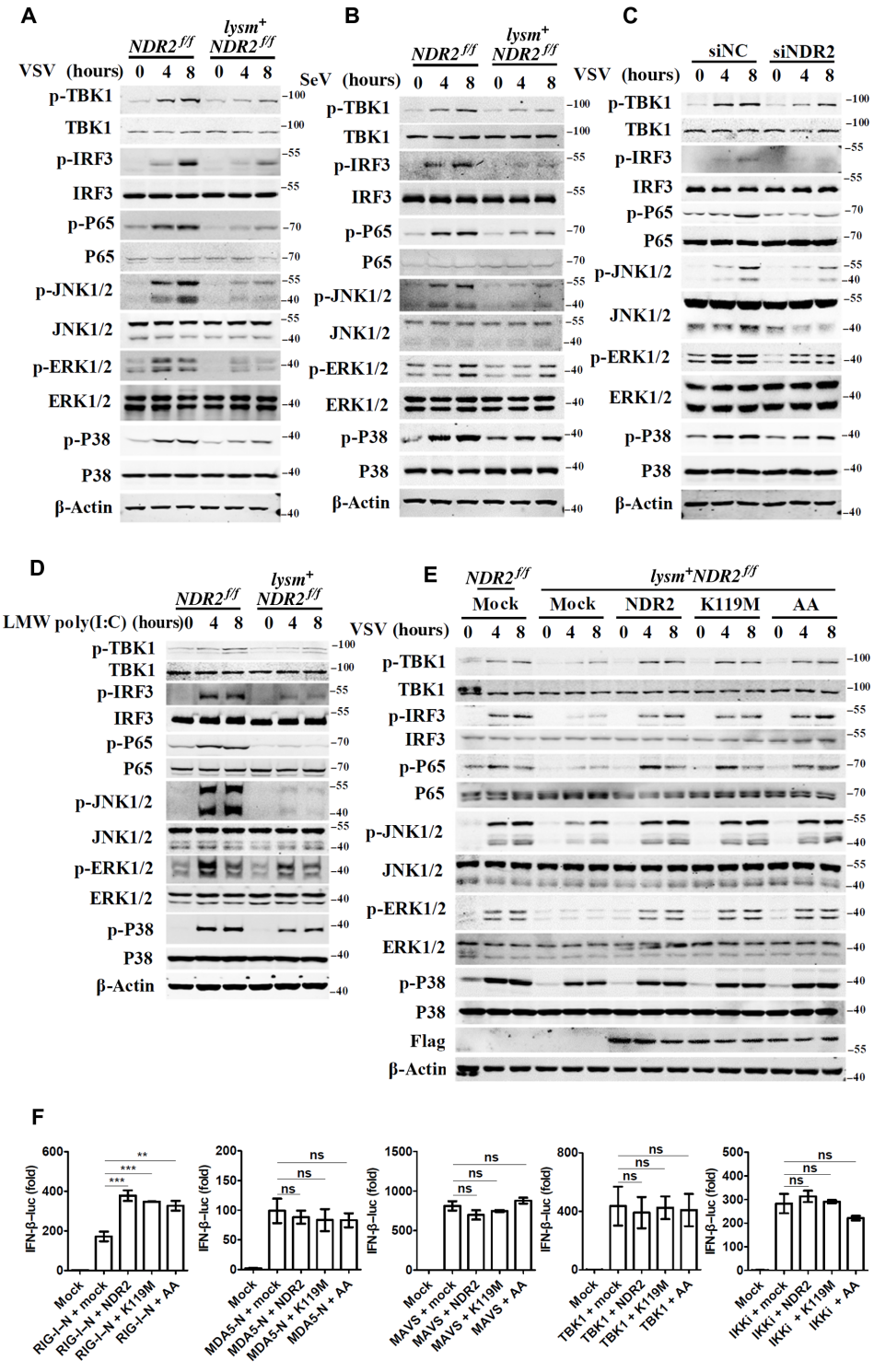


**Fig. 3. NDR2 specifically promotes RIG-I pathway activation in a kinase-independent manner.** (**A** and **B**) *NDR2*$^{f/f}$ and *Lysm*$^{+}$*NDR2*$^{f/f}$ PMs were infected with VSV (A) or SeV (B) for the indicated times, and then, immunoblotting analysis was performed to detect the total and phosphorylated (p-) TBK1, IRF3, P65, ERK1/2, JNK1/2, and P38. (**C**) BMDMs were transfected with NDR2-specific or scrambled small interfering RNA (siRNA), followed by VSV infection for the indicated periods, and then, immunoblotting analysis was performed to detect the total and phosphorylated TBK1, IRF3, P65, ERK1/2, JNK1/2, and P38. (**D**) *NDR2*$^{f/f}$ and *Lysm*$^{+}$*NDR2*$^{f/f}$ PMs were transfected with LMW poly(I:C) (1 μg ml$^{-1}$) for the indicated times, and then, immunoblotting analysis was performed to detect the total and phosphorylated TBK1, IRF3, P65, ERK1/2, JNK1/2, and P38. (**E**) *NDR2*$^{f/f}$ and *Lysm*$^{+}$*NDR2*$^{f/f}$ PMs were transfected with vectors expressing NDR2 or its kinase-inactive mutants for 36 hours, followed by infection with VSV to detect the total and phosphorylated TBK1, IRF3, P65, ERK1/2, JNK1/2, and P38 by immunoblotting. (**F**) Human embryonic kidney (HEK) 293 cells were transfected with RIG-I CARDs (caspase activation and recruitment domains), MDA5 CARDs, MAVS, TBK1, and IKKi, along with IFN-β reporter plasmid and NDR2 or its kinase-inactive mutant vectors for 48 hours, and luciferase activity was analyzed. Data are means ± SD and are representative of three independent experiments. Student's *t* test was used for statistical calculation. $^{**}P < 0.01$ and $^{***}P < 0.001$.

mutants promoted IFN-β and IRF3 reporter activation induced by RIG-I–N [as a constitutively active RIG-I mutant containing the N-terminal caspase activation and recruitment domains (CARDs) of RIG-I], whereas it had no apparent effect on MDA5-N– (as a constitutively active MDA5 mutant containing the N-terminal CARDs of MDA5), MAVS-, TBK1-, or IKKi (IκB kinase epsilon)–induced IFN-β (Fig. 3F) and IRF3 (fig. S3E) reporter activation. Consistent with data that NDR2 has no effect on the anti-DNA virus immune response, NDR2 did not affect STING (stimulator of interferon gene)–induced IFN-β (fig. S3F) and IRF3 (fig. S3G) reporter activation. Collectively, these data suggest that NDR2 positively modulates RIG-I–mediated signaling by targeting at the RIG-I level in a kinase-independent manner.

### NDR2 interacts with RIG-I and enhances its K63-linked polyubiquitination

To investigate the underlying mechanisms involved in the positive regulation of the RIG-I signaling pathway by NDR2, we immunoprecipitated exogenous NDR2 from lysates of RAW264.7 macrophages stably overexpressing Flag-tagged NDR2 using anti-Flag mouse magnetic (M2) beads, as an anti-NDR2 antibody does not work for immunoprecipitation (IP) assays. As shown in Fig. 4A, NDR2 interacted with RIG-I at the basal level, which peaked at 4 hours after VSV infection. However, NDR2 did not interact with endogenous MAVS, TBK1, or IRF3 in RAW264.7 macrophages (Fig. 4A). Transient transfection and coimmunoprecipitation experiments in human embryonic kidney (HEK) 293 cells showed that Myc-NDR2 interacted with Flag–RIG-I but not Flag-tagged MAVS, TBK1, or IKKi (Fig. 4B). Furthermore, an endogenous protein IP assay with anti–RIG-I antibody in PMs infected with or without VSV showed that endogenous RIG-I interacted with endogenous NDR2, but not with NDR1, at the basal level, which peaked at 4 hours and reverted to the basal level at 8 hours after VSV infection in PMs (Fig. 4C).

NDR2 consists of a central kinase catalytic domain, which is flanked with N- and C-terminal regulatory domains (*22*). To determine which domain of NDR2 was required for its interaction with RIG-I, we constructed the different deletion constructs of NDR2, and domain-mapping experiments showed that RIG-I interacts with the central kinase catalytic domain of NDR2 (NDR2 STKc) (Fig. 4D and fig. S4A). We also determined that the CARDs of RIG-I is necessary for its association with NDR2 (Fig. 4E and fig. S4B). Collectively, these data indicate that NDR2 interacts with the CARDs of RIG-I via its STKc domain.

Modification of K63-linked polyubiquitination in the CARDs of RIG-I is required for its activation and downstream signal transduction (*2*). We next explored whether NDR2 affected the ubiquitination of RIG-I. Flag-tagged RIG-I and hemagglutinin (HA)–tagged ubiquitin-expressing plasmids were transfected into HEK293 cells in the absence or presence of Myc-NDR2. Then, Flag–RIG-I was immunoprecipitated, and ubiquitination of RIG-I was detected with an anti-HA antibody. As shown in Fig. 4F, NDR2 significantly increased total ubiquitination of RIG-I in a dose-dependent fashion. Moreover, the NDR2 kinase–inactive mutants promoted RIG-I ubiquitination as efficiently as WT NDR2 (Fig. 4G), indicating that NDR2 positively modulates RIG-I ubiquitination in a kinase activity–independent manner. To verify which form of the polyubiquitin chains of RIG-I is regulated by NDR2, we cotransfected plasmids into HEK293 cells expressing HA-tagged ubiquitin or the mutant ubiquitin HA–K11R ub, HA–K29R ub, HA–K48R ub, or HA–K63R ub together with Myc-NDR2 and Flag-RIG-I. As shown in Fig. 4H, transfection with HA–K63R ub abolished the effect of NDR2 on the ubiquitination of RIG-I. Furthermore, NDR2 deficiency inhibited total and K63-linked polyubiquitination of endogenous RIG-I in BMDMs during virus infection (Fig. 4I). Together, these results suggest that NDR2 promotes K63-linked polyubiquitination of RIG-I.

### NDR2 promotes TRIM25-mediated RIG-I K63-linked ubiquitination

TRIM25, Riplet, and TRIM4 mediate K63-linked polyubiquitination of RIG-I and modulate RIG-I–mediated signaling (*5*–*7*). To unveil the underlying mechanism by which K63-linked polyubiquitination of RIG-I is regulated by NDR2, we performed transient transfection and coimmunoprecipitation experiments in HEK293 cells. As shown in Fig. 5A, NDR2 selectively interacted with TRIM25 but not with the other two E3 ubiquitin ligases, Riplet and TRIM4. The recombinant proteins of Flag–RIG-I, Flag-TRIM25, and Myc-NDR2 were purified in HEK293 cells, and a protein pull-down assay was performed using anti-Flag M2 beads. Both Flag–RIG-I and Flag-TRIM25 were able to pull down Myc-NDR2 (Fig. 5B), indicating that NDR2 directly interacted with RIG-I and TRIM25. Confocal microscopy experiments also showed that Myc-NDR2 colocalized with the exogenous Flag-TRIM25 in the cytoplasm of HEK293 cells (fig. S5A). Furthermore, NDR2, but not NDR1, physically interacted with TRIM25, and SeV infection increased the interaction in HEK293 cells (Fig. 5C). TRIM25 consists of an N-terminal catalytic RING domain, two B-box domains, a coiled-coil dimerization domain (CCD), and a C-terminal SPRY domain (*23*). As shown in fig. S5B, NDR2 interacts with the Flag-CCD but not with a CCD domain–deficient deletion construct Flag-$^{\triangle}$CCD, indicating that the CCD domain is required for mediating the interaction of TRIM25 with NDR2. Moreover, domain-mapping experiments showed that the N-terminal regulatory domain of NDR2 is essential for its interaction with TRIM25 (fig. S5C). Overexpression of NDR2 increased the interaction between TRIM25 and RIG-I (Fig. 5D) and enhanced the exogenous TRIM25-mediated K63-linked ubiquitination of RIG-I (fig. S5D). The ability of NDR2 to regulate TRIM25-mediated RIG-I ubiquitination was further investigated by an in vitro ubiquitin ligase activity assay. As shown in Fig. 5E, TRIM25 recombinant protein catalyzed the ubiquitination of RIG-I in vitro. Addition of a full-length NDR2 recombinant protein, but not its mutants (NDR2 dN and NDR2 dSTKc) that no longer bound to RIG-I or TRIM25, significantly facilitated TRIM25-mediated RIG-I ubiquitination. To further demonstrate whether NDR2 promotes RIG-I ubiquitination via TRIM25, TRIM25-deficient HEK293 cells were generated using the CRISPR-Cas9 system (fig. S5, E and F). TRIM25 deficiency in HEK293 cells not only impaired RIG-I ubiquitination but also abolished the promoting effect of NDR2 on RIG-I ubiquitination, which was rescued to a level comparable to WT HEK293 cells with overexpression of Myc-TRIM25 (fig. S5G).

We further investigated whether NDR2 that promotes the antiviral innate immune response depended on enhancing TRIM25-mediated RIG-I ubiquitination in TRIM25 knockout (TRIM25$^{-/-}$) L929 cells (a mouse fibroblast cell line) (fig. S5, H and I). Overexpression of NDR2 promoted VSV-induced total and K63-linked polyubiquitination of RIG-I in L929 cells, but this phenomenon was abolished in TRIM25$^{-/-}$ L929 cells (Fig. 5F). NDR2 overexpression consistently promoted VSV-induced IFN-β, IL-6, and TNF-α production and inhibited virus replication in control L929 cells, which also disappeared

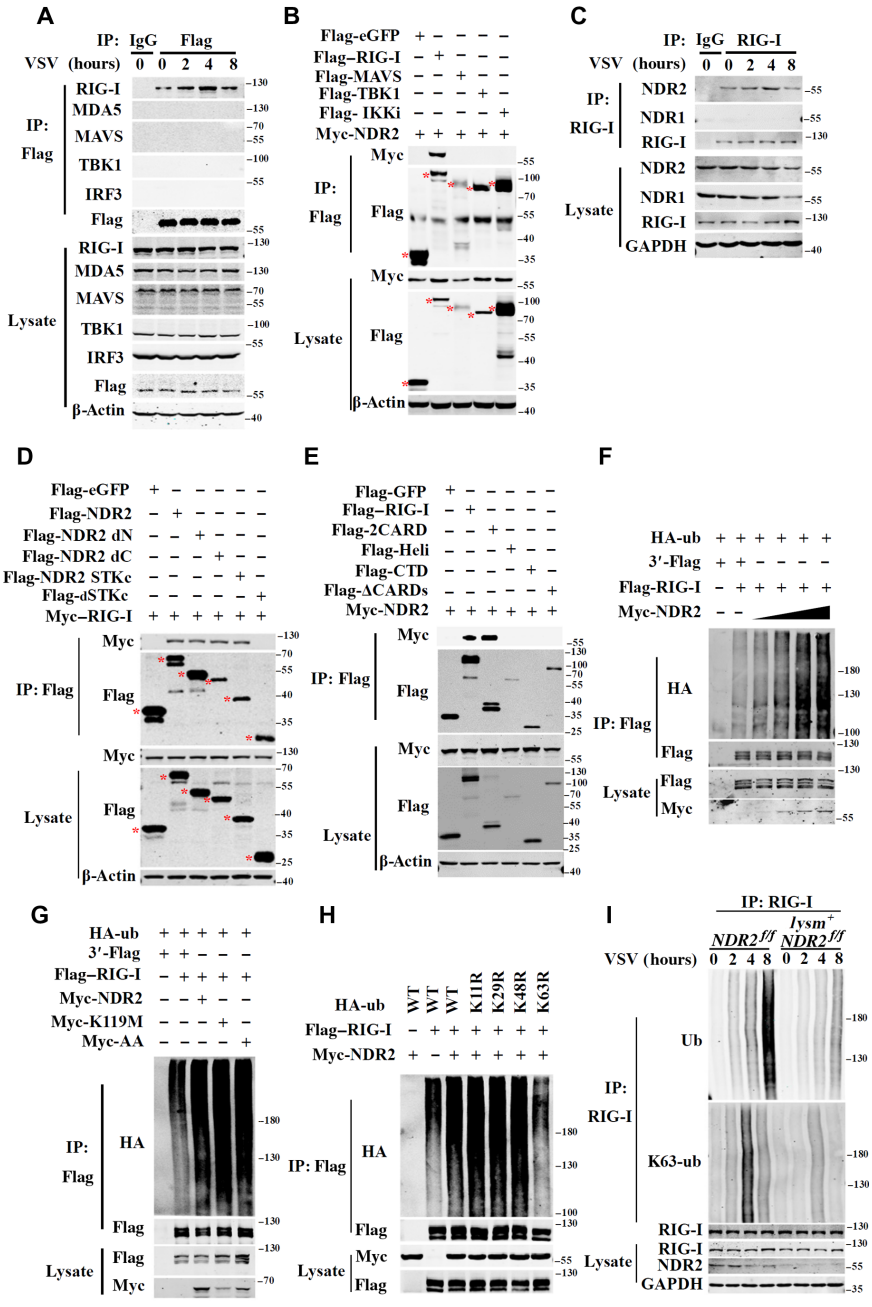


**Fig. 4. NDR2 interacts with RIG-I and promotes RIG-I K63-linked polyubiquitination.** (**A**) Immunoblot analysis of extracts of RAW264.7 macrophages stably overexpressing Flag-NDR2 and infected with VSV for the indicated times was performed, and then, whole-cell lysates were immunoprecipitated with anti-Flag mouse magnetic (M2) beads, followed by immunoblotting with the indicated antibodies. (**B**) Flag-tagged RIG-I, MAVS, TBK1, or IKKi was coexpressed with Myc-NDR2 in HEK293 cells, followed by IP with anti-Flag M2 beads, followed by immunoblotting with anti-Flag or anti-Myc antibodies. (**C**) Lysates from murine PMs infected with VSV for the indicated time periods were subjected to IP with anti–RIG-I antibody, followed by Western blot analysis with the indicated antibodies. GAPDH, glyceraldehyde-3-phosphate dehydrogenase. (**D**) Flag-tagged full-length NDR2(1–464), dN(90–464), dC(1–383), dNC(90–383), or dS-TKc truncation mutants were coexpressed with Myc–RIG-I in HEK293 cells, and whole-cell lysates were immunoprecipitated with anti-Flag M2 beads, followed by immunoblotting with anti-Flag or anti-Myc antibodies. (**E**) Flag-tagged full-length RIG-I(1–926), 2CARD(1–233), Heli(234–734), CTD(735–926), or dCARD(234–926) truncation mutants were coexpressed with Myc-NDR2 in HEK293 cells, and whole-cell lysates were immunoprecipitated with anti-Flag M2 beads, followed by immunoblotting with anti-Flag or anti-Myc antibodies. (**F**) Immunoblot analysis of the polyubiquitination of RIG-I in HEK293 cells cotransfected with Flag–RIG-I, hemagglutinin (HA)–ubiquitin (HA-ub), and increasing concentrations (wedge) of vectors for the Myc-NDR2 constructs, followed by denaturation-IP with anti-Flag M2 beads and immunoblot analysis with an anti-HA antibody. (**G**) Immunoblot analysis of the polyubiquitination of RIG-I in HEK293 cells cotransfected with Flag–RIG-I, HA-ubiquitin, and Myc-NDR2 or its kinase-inactive mutant constructs, followed by denaturation-IP with anti-Flag M2 beads and immunoblot analysis with anti-HA antibodies. (**H**) Immunoblot analysis of the ubiquitination of RIG-I in HEK293 cells cotransfected with Flag–RIG-I, Myc-NDR2, and HA-ub or the mutant ubiquitin constructs, followed by denaturation-IP with anti-Flag M2 beads and immunoblot analysis with anti-HA antibodies. (**I**) *NDR2*$^{f/f}$ and *Lysm*$^{+}$*NDR2*$^{f/f}$ BMDMs were infected with or without VSV for the indicated periods. Cell lysates were immunoprecipitated with anti–RIG-I, and the immunoprecipitates were analyzed by immunoblots with the indicated antibodies.

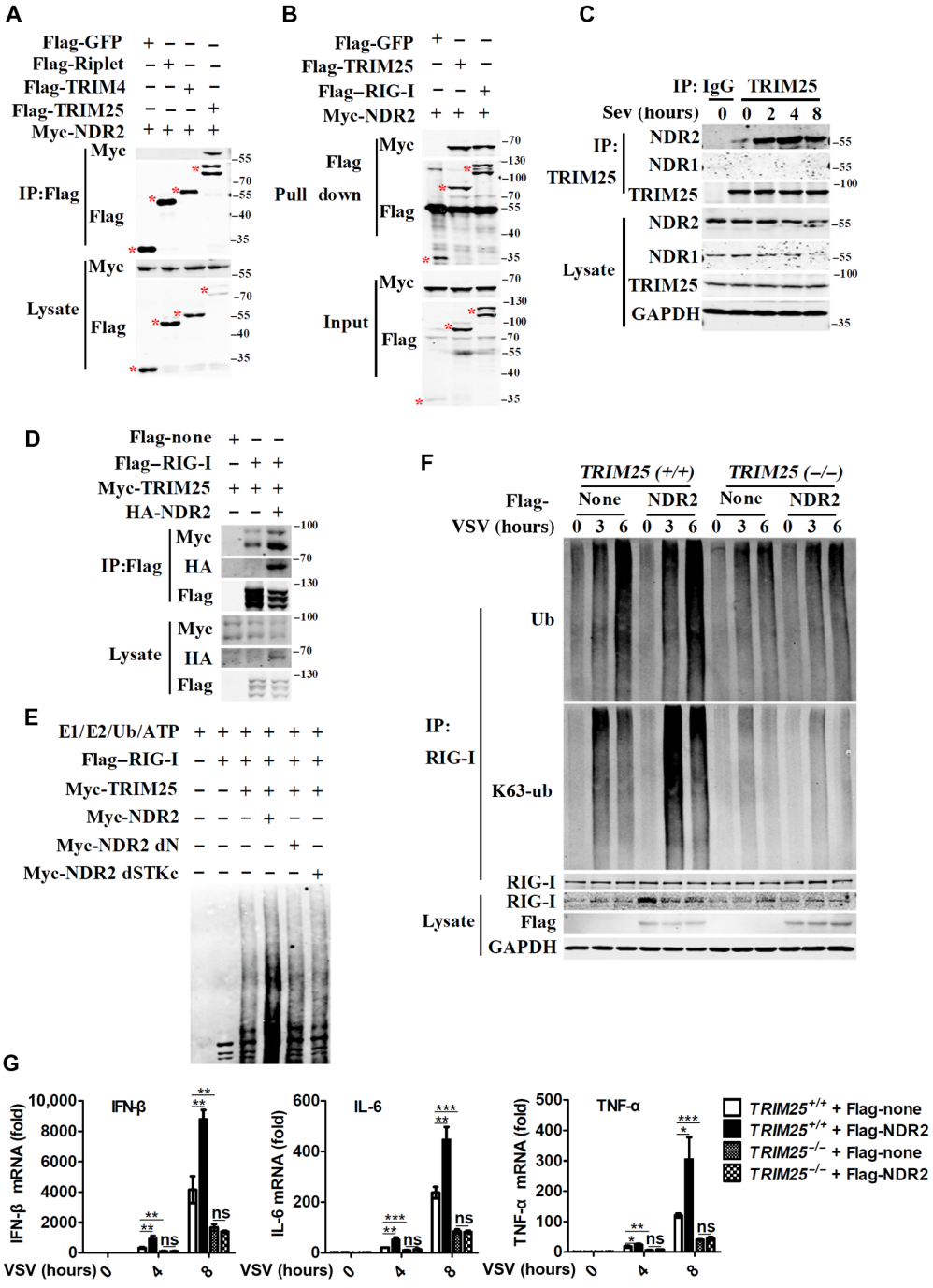


**Fig. 5. NDR2 enhances TRIM25-mediated RIG-I K63-linked ubiquitination via facilitating recruitment of TRIM25 to RIG-I.** (**A**) Flag-tagged Riplet, TRIM4, or TRIM25 were coexpressed with Myc-NDR2 in HEK293 cells, and then, whole-cell lysates were immunoprecipitated with anti-Flag M2 beads, followed by immunoblotting with anti-Flag or anti-Myc antibodies. (**B**) Recombinant Myc-tagged NDR2 proteins were mixed with Flag-tagged GFP-, TRIM25-, or RIG-I–purified proteins. The proteins were then pulled down with anti-Flag M2 beads, followed by immunoblotting with anti-Flag or anti-Myc antibodies. (**C**) Lysates from HEK293 cells infected with SeV for the indicated time were immunoprecipitated with anti-TRIM25 antibodies, followed by Western blot analysis with the indicated antibodies. IgG, immunoglobulin G. (**D**) IP and immunoblot analysis of HEK293 cells transfected with the indicated combinations of plasmids encoding HA-NDR2, Flag–RIG-I, and Myc-TRIM25. Then, whole-cell lysates were immunoprecipitated with anti-Flag M2 beads, followed by immunoblotting with anti-Flag, anti-Myc, or anti-HA antibodies. (**E**) Recombinant RIG-I, TRIM25, NDR2, NDR2 dN, NDR2 dSTKc, and ubiquitination-associated proteins were mixed in adenosine 5′-triphosphate buffer and incubated at 30°C for 2 hours. Then, reaction aliquots were quenched and evaluated by SDS–polyacrylamide gel electrophoresis (SDS-PAGE) and immunoblotting. (**F**) Immunoblot analysis of the polyubiquitination of RIG-I in WT and *TRIM25*-deficient L929 cells transfected with empty vector or Flag-NDR2 plasmids. Thirty-six hours later, the cells were infected with VSV for the indicated times, followed by denaturation-IP with anti–RIG-I and immunoblot analysis with the indicated antibodies. (**G**) Real-time PCR analysis of IFN-β, IL-6, and TNF-α mRNA in WT and *TRIM25*-deficient L929 cells transfected with plasmids encoding Flag-NDR2 or empty vector for 24 hours, followed by VSV infection for the indicated periods. Data are means ± SD and are representative of three independent experiments. Student's *t* test was used for statistical calculation. **P* < 0.05, ***P* < 0.01, and ****P* < 0.001.

in TRIM25$^{-/-}$ L929 cells (Fig. 5G and fig. S5, J to L). Silencing NDR2 facilitated virus replication and restrained VSV-induced IFN-β, IL-6, and TNF-α expression in the control L929 cells but not in TRIM25$^{-/-}$ L929 cells (fig. S5, M to O). Together, these data indicate that NDR2 associates directly with TRIM25 and RIG-I to promote TRIM25-mediated RIG-I ubiquitination, which is required for RIG-I–mediated downstream signal transduction and type I IFN amplification.

### Viral infection suppresses NDR2 expression in a type I IFN pathway–dependent manner

On the basis of publicly available gene array data (Gene Expression Omnibus profiles GSE68849 and GSE6489), NDR2 transcripts are down-regulated in primary plasmacytoid dendritic cells and primary pulmonary microvascular cells with virus infections (fig. S6A). We collected peripheral blood samples from 77 cases of pediatric patients infected with RSV and 40 healthy controls and detected the NDR2 mRNA level in PBMCs. Compared to the healthy group, NDR2 expression was sharply decreased in PBMCs from the RSV-infected group (Fig. 6A). Furthermore, infection of RNA viruses (VSV, H1N1, SeV, or RSV) or DNA viruses (HSV-1 or MHV68) significantly down-regulated NDR2 expression in PMs (Fig. 6, B and C). Consistently, VSV infection markedly reduced NDR2 expression in human primary PBMCs and acute monocytic leukemia cell line Thp1 cells (fig. S6, B and C).

We next explored whether NDR2 was restrained by signaling events upstream of IFN production or downstream of the IFN/JAK/STAT1 effector signaling pathway. Recombinant type I IFN treatment markedly down-regulated NDR2 expression in PMs (Fig. 6D and fig. S6D) and Thp1 cells (Fig. 6E and fig. S6E). However, VSV infection did not down-regulate NDR2 expression in IFNαR- or STAT1-deficient immortalized BMDMs (Fig. 6F and fig. S6F), suggesting that IFNαR-STAT1 signaling is required for the down-regulation of NDR2 in macrophages during virus infection.

A number of histone modifications are associated with the transcriptional regulation of genes and RNA polymerase elongation in the transcribed region. In the histone H3 tail, there are four lysine residues that are methylated in chromatin, including K4, K9, K27, and K36. It is generally accepted that K4 and K36 are methylated in transcriptionally active chromatin, whereas methylation of K9 and K27 is linked with inactive chromatin (*24*). A chromatin IP (ChIP) assay showed that H3K27me3 (tri-methylation occurring on the K27 residue of the core histone H3) was enhanced in the NDR2 promoter region in Thp1 cells after treatment with VSV or IFN-α (Fig. 6G). However, VSV infection or IFN-α stimulation had no effect on H3K4me3 modification in the promoter of NDR2 (Fig. 6H). Together, these data indicate that NDR2 expression is down-regulated in virus-infected innate immune cells mainly through the IFN/JAK/STAT1 signaling pathway and enhances H3K27me3 modification in the NDR2 promoter.

## DISCUSSION

In the current study, we determined that NDR2 participates in the RIG-I–mediated antiviral innate immune response. NDR2 directly associates with RIG-I and TRIM25 to facilitate the recruitment of TRIM25 to RIG-I, leading to enhanced TRIM25-mediated K63-linked polyubiquitination of RIG-I, which ultimately results in the up-regulation of RIG-I activation and downstream antiviral signaling. We further identified that virus infection repressed NDR2 expression via the type I IFN pathway.

NDR2 is a highly conserved serine/threonine kinase in the NDR/LATS kinase family. Here, we demonstrated that NDR2 plays important roles in defending against the invasion of RIG-I–sensing RNA viruses but not of DNA viruses in mice. NDR2 knockout or knockdown markedly attenuated the production of type I IFNs and inflammatory cytokines in macrophages upon RIG-I–sensing RNA virus infection, whereas overexpression of NDR2 or its kinase-inactive mutants enhanced RIG-I–sensing RNA virus infection–induced type I IFNs and inflammatory cytokine expression. Consistently, we observed more viral replication in NDR2-deficient PMs than in WT PMs. In line with the promoting effect of NDR2 on the anti–RIG-I–sensing RNA virus immune response in vitro, NDR2 deficiency also specifically rendered mice more susceptible to RIG-I–sensing RNA virus infection.

Upon RIG-I–sensing RNA virus invasion, viral double-stranded RNAs are sensed by RIG-I, which is activated and binds to MAVS, leading to NF-κB, MAPK, and IRF pathway activation (*3*). In the present study, we demonstrated that NDR2 promotes the RIG-I–induced activation of NF-κB, MAPK, and IRF pathways in a kinase-independent manner. We further identified that NDR2 binds to RIG-I and TRIM25 and enhances TRIM25-mediated RIG-I K63-linked ubiquitination, which is required for downstream antiviral signaling activation. Correspondingly, TRIM25 deficiency abolishes the promoting effect of NDR2 on virus clearance.

NDR1 and NDR2 are ubiquitously expressed in human tissues (*25*). NDR1 predominantly accumulates within the nucleus via a non-consensus nuclear localization signal in its catalytic domain (*26*). Our recent study demonstrated that NDR1, as a transcriptional regulator in the nucleus, directly binds to the intergenic region of miR146a and inhibits NF-κB–mediated miR146a transcription, thereby leading to potentiated STAT1 translation. NDR1, as a positive regulator of ISG induction, plays an essential role in defending against both DNA and RNA virus infection.

In contrast to the nuclear distribution exhibited by NDR1, NDR2 is mostly excluded from the nucleus and exhibits a punctate cytoplasmic distribution (*12*). Here, we demonstrated that NDR2 acts as a scaffolding protein, assisting in the interaction between TRIM25 and RIG-I in the cytoplasm, which results in enhanced RIG-I K63-linked polyubiquitination and activation. Therefore, NDR2 selectively protects mice from RIG-I–sensing RNA virus invasion. While an extremely high degree of sequence identity is observed between these two kinases, the differential localization of NDR1 and NDR2 leads to the fact that each kinase serves distinct functions in antiviral innate immune responses.

NDR2 can act as a tumor suppressor, and its reduced gene expression has been reported in many types of human cancers (*12*). Here, we found that the NDR2 transcripts were decreased in PBMCs from pediatric patients infected with RSV compared with those from healthy children, implying that NDR2 expression might correlate with antiviral immunity in humans. Our previous study showed that the NDR1 transcript is also suppressed upon viral infection depending on IFN/JAK/STAT1 signaling. We observed up-regulated H3K27me3 modification in both NDR1 and NDR2 promoter regions in Thp1 cells after VSV infection, indicating that mechanisms underlying the regulation of NDR1 and NDR2 expression might be conserved in macrophages during virus infection. The down-regulation of NDR1 and NDR2 might be a negative feedback mechanism of the host immune response for virus infection. Devroe *et al.* (*15*) reported that NDR1/2 kinases were incorporated into HIV-1 particles and

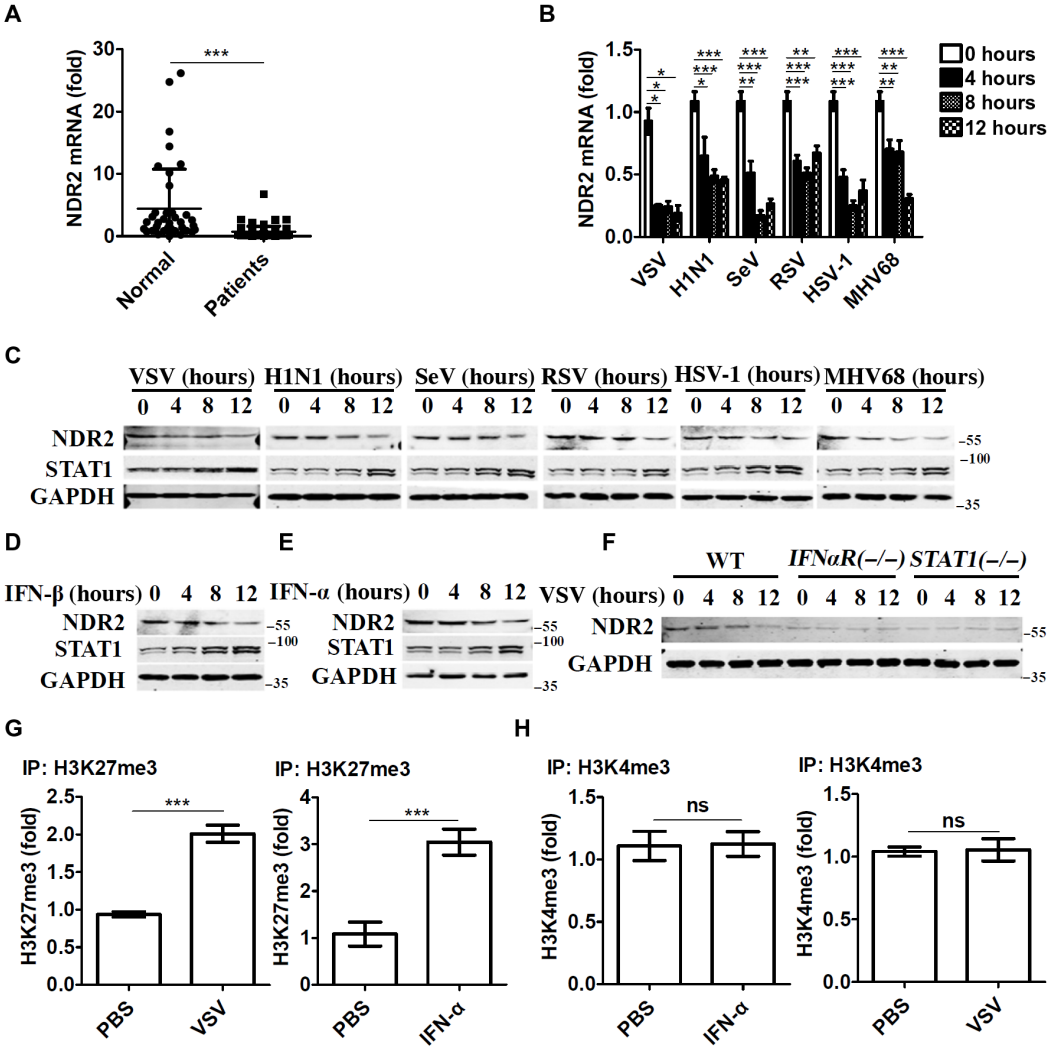


**Fig. 6. Viral infection dampens NDR2 expression in an IFN/STAT1-dependent manner.** (**A**) NDR2 expression in PBMCs from RSV-infected patients ($n = 77$) and healthy controls ($n = 40$) was analyzed by real-time PCR analysis. (**B** and **C**) NDR2 expression in PMs infected with RNA viruses (VSV, H1N1, SeV, and RSV) or DNA viruses (HSV-1 and MHV68) for the indicated periods was detected by real-time PCR (B) and immunoblotting (C). STAT1 expression was detected to ensure that the antiviral immune response was triggered in the virus-infected cells. (**D** and **E**) NDR2 expression in PMs stimulated with murine recombinant IFN-β (100 IU ml$^{-1}$) (D) or in Thp1 cells stimulated with human recombinant IFN-α (100 IU ml$^{-1}$) (E) for the indicated times was detected by immunoblotting. (**F**) WT, *IFNαR*$^{-/-}$, or *STAT1*$^{-/-}$ immortalized BMDMs were infected with VSV for the indicated periods, followed by immunoblotting analysis of NDR2 expression. (**G** and **H**) H3K27me3 (G) and H3K4me3 (H) modifications were detected by chromatin IP (ChIP)–quantitative PCR on *NDR2* gene promoter loci in the lysates of Thp1 cells infected with VSV for 8 hours or with IFN-α (100 IU ml$^{-1}$) for 4 hours. Data are means ± SD and are representative of three independent experiments. Student's *t* test was used for statistical calculation. *$P < 0.05$, **$P < 0.01$, and ***$P < 0.001$.

suffered cleavage and enzymatic activity inhibition by the HIV-1 PR. However, we analyzed the whole genome of VSV (GenBank: J02428.1) in the National Center for Biotechnology Information database and did not find any gene that encodes PR in VSV. Moreover, we did not detect any cleavaged NDR2 protein in the lysate of macrophages infected with VSV by Western blot (Fig. 6C).

In summary, our data have demonstrated that NDR2 positively regulated an antiviral innate immune response in a kinase activity–independent manner. NDR2 interacts with RIG-I and promotes TRIM25-mediated RIG-I ubiquitination, which is required for downstream signaling activation and type I IFN production. We further showed that virus infection down-regulated NDR2 expression through the IFN/JAK/STAT1 signaling pathway. These findings not only provide insights into the positive regulation of RIG-I-mediated antiviral innate immune responses but also provide a negative feedback mechanism underlying host immunological response in macrophages.

## MATERIALS AND METHODS

### Mice

NDR2$^{f/f}$ mice, a C57BL/6J background, were gifts from B. Hemmings (Friedrich Miescher Institute for Biomedical Research). Lysm-Cre mice C57BL/6J were provided by L. Wang (Zhejiang University School of Medicine). Mice genotype identification was performed by polymerase chain reaction (PCR) analysis of DNA isolated from the tail using the following primers: NDR2-F, 5′-CCTCAGACTTTTTGTGATCCTCC-3′; NDR2-R, 5′-AGCTCAACCTCCCAACTCAG-3′; Lysm-mut, 5′-CCAGAAATGCCAGATTACG-3′; Lysm-com, 5′-CTTGGGCTGCCAGAATTTCTC-3′; and Lysm-wt,

5′-TTACAGTCGGCCAGGCTGAC-3′. All mice were maintained under specific pathogen–free conditions in the University Laboratory Animal Center. All animal experiments were approved by the Ethical Review Committee of Zhejiang University School of Medicine and were in compliance with institutional guidelines.

### Cell culture and reagents

HEK293, L929, Thp1, and RAW264.7 cells were obtained from the American Type Culture Collection (Manassas, VA). IFNαR- and STAT1-deficient immortal BMDMs were gifts from G. Cheng (University of California, Los Angeles). Thioglycolate (Merck)–elicited mouse PMs were cultured in RPMI-1640 medium (Invitrogen) with 10% heat-inactivated fetal bovine serum (FBS) (Biological Industries), penicillin (100 U $ml^{-1}$) (Beyotime), and streptoMycin (100 μg $ml^{-1}$) (Beyotime). BMDMs were generated from the bone marrow of 8-week-old female mice. Bone marrow cells were collected from the femurs and tibias of mice, and BMDMs were differentiated in RPMI-1640 medium (Invitrogen) with 10% heat-inactivated FBS (Biological Industries), penicillin (100 U $ml^{-1}$) (Beyotime), streptoMycin (100 μg $ml^{-1}$) (Beyotime), and recombinant mouse macrophage colony-stimulating factor (20 ng $ml^{-1}$) (PeproTech). Mouse recombinant IFN-β and human recombinant IFN-α were purchased from PeproTech. LMW and HMW poly(I:C) and anti-Flag mouse magnetic (M2) beads were from Sigma-Aldrich.

### Plasmid constructs and transfection

The Flag-NDR2 plasmid was provided by Z. Xia (Life Sciences Institute, Zhejiang University, Hangzhou) and was subcloned into the pcDNA3.1 eukaryotic expression vector (Invitrogen). The Flag–RIG-I was provided by X. Cao (Second Military Medical University, Shanghai). The Myc-MDA5 CARDs plasmid was provided by W. Zhao (Shandong University, Jinan). The TRIM25 plasmids were provided by P. Wang (Tongji University, Shanghai). Then, mutant expression plasmids for NDR2 (K119M, S282A T442A, dN, dC, dNC, and dSTKc), RIG-I [CARDs, Heli, CTD (C-terminal domain), and dCARD], and TRIM25 (RING, B-box/CCD, CCD, dCCD, and SPRY) were generated using the KOD-Plus-Neo Kit (Toyobo). The Flag-TRIM4 plasmid was provided by H. Shu (Wuhan University, Wuhan). The Flag-Riplet plasmid was provided by D. Chen (Peking University, Beijing). The HA-tagged WT and mutant ubiquitin plasmids were provided by H. An (Second Military Medical University, Shanghai). All constructs were confirmed by DNA sequencing (GENEWIZ). Plasmids were transfected into murine PMs with Lipofectamine 3000 (Invitrogen) according to the manufacturer's protocol. JetPRIME reagent (Polyplus) was used to transfect plasmids into RAW264.7 stable cell lines according to the manufacturer's protocol and then selected with puroMycin (8 μg $ml^{-1}$) (Sigma-Aldrich), and single-cell colony cells were picked and validated by immunoblotting. Polyethylenimine (Polysciences) was used for HEK293 cells transfection with plasmids. LMW and HMW poly(I:C) was transfected into PMs with INTERFERin reagent (Polyplus) according to a standard protocol. Small interfering RNA (siRNA)–targeted mouse NDR2 was purchased from Thermo Fisher Scientific, and other siRNA duplexes were synthesized from GenePharma. The siRNA duplexes were transfected into human PBMCs, PMs, and L929 cells with INTERFERin reagent (Polyplus) according to a standard protocol. The sequences of siRNAs used in this study were as follows: 5′-UUCUCCGAACGUGUCACGU-3′ (control siRNA) and 5′-GGAUAAGAGGAAUCUUUAUTT-3′ (siRNA for human NDR2).

### Virus infection and titer

Viruses were propagated, as described previously (*27*). Cells were infected with H1N1 [multiplicity of infection (MOI) = 1], SeV (MOI = 10), RSV (MOI = 1), MHV68 (MOI = 5), HSV-1 (MOI = 5), VSV (MOI = 0.1), EMCV (MOI = 10), VSV-GFP (green fluorescent protein) (MOI = 1), and HSV-eGFP (enhanced GFP) (MOI = 5) for the indicated times. For in vivo studies, 8-week-old male littermate mice were intraperitoneally injected with VSV [$1 \times 10^7$ plaque-forming units (PFU) $g^{-1}$, 12 hours] for the determination of cytokine production in serum, PMs, and the spleen and of viral titers in organs. For $TCID_{50}$ assay, $1 \times 10^4$ cells were seeded into 96-well plates 1 day before measurement. Then, cell culture supernatant or tissue homogenate with VSV infection was serially diluted on the monolayer of HEK293 cells for 3 to 7 days, and $TCID_{50}$ was measured. For in vivo survival studies, 8-week-old male littermate mice were infected intravenously with VSV ($1 \times 10^8$ PFU $g^{-1}$) or intranasally with H1N1 ($2 \times 10^3$ PFU per mouse). For HSV-1 infection in vivo, HSV-1 ($1 \times 10^6$ PFU per mouse) was injected intravenously into 8-week-old male littermate mice for the determination of cytokine production in serum (6 hours), viral load in brain (4 days), and overall survival assay.

### IP and immunoblot analysis

For IP, whole-cell extracts were lysed in IP buffer, as described previously (*16*), and in a protease inhibitor cocktail (Sigma-Aldrich). After centrifugation for 10 min at 12,000*g* at 4°C, supernatants were collected and incubated with protein G magnetic beads (Bio-Rad) together with corresponding antibodies. After overnight incubation, the beads were washed three times with IP buffer. Immunoprecipitates were eluted by boiling with 1% (w/v) SDS sample buffer. For immunoblot analysis, cells were lysed with cell lysis buffer (Cell Signaling Technology) supplemented with a protease inhibitor cocktail (Sigma-Aldrich). Protein concentrations in the extracts were measured with a BCA (bicinchoninic acid) protein assay kit (Pierce) and were made equal with an extraction reagent. Immunoprecipitates or whole-cell lysates were loaded and subjected to SDS–polyacrylamide gel electrophoresis (PAGE), transferred onto nitrocellulose membranes, blocked with 5% dry nonfat milk in tris-buffered saline (pH 7.4) containing 0.1% Tween 20, and then blotted with the indicated antibodies, which are listed in table S1.

### Protein ubiquitination analysis

For exogenous RIG-I ubiquitination analysis, HEK293 cells were transfected with plasmids expressing RIG-I, TRIM25, NDR2, and ubiquitin for at least 24 hours. For endogenous RIG-I ubiquitination analysis, immortalized BMDMs or L929 cells were treated with VSV for the indicated times. Then, cells were lysed and boiled for 5 min in IP buffer supplemented with 1% SDS. The cell lysate was diluted to 0.1% SDS with IP buffer. After centrifugation for 10 min at 12,000*g* at 4°C, supernatants were collected and incubated with protein G magnetic beads (Bio-Rad) together with corresponding antibodies. After overnight incubation, the beads were washed three times with IP buffer. Immunoprecipitates were eluted by boiling with 1% (w/v) SDS sample buffer and used for immunoblot analysis. The in vitro ubiquitination assay was described previously (*28*). Briefly, recombinant RIG-I, TRIM25, NDR2, and ubiquitination-associated proteins were mixed in adenosine 5′-triphosphate buffer. All tubes were incubated at 30°C for 2 hours and stopped by the addition of denaturing sample buffer followed by 95°C treatment for 5 min. Samples were resolved on 6% SDS-PAGE and analyzed by immunoblotting with an anti-ubiquitin antibody.

### Enzyme-linked immunosorbent assay

The protein levels of murine IFN-β, IL-6, and TNF-α in cell culture supernatants and sera were detected by enzyme-linked immunosorbent assay (ELISA) according to the manufacturers' instructions (BioLegend and eBioscience).

### Quantitative reverse transcription PCR

Total RNA was isolated from cells using TRIzol reagent (Life Technologies) according to the manufacturer's directions. Single-strand complementary DNA was generated from total RNA and reverse transcription. The SYBR Green master Rox (Vazyme) were used for quantitative real-time reverse transcriptase PCR analysis on a CFX Touch system (Bio-Rad). The sequences for primers are listed in table S2.

### Generation and validation of TRIM25 knockout cells

The TRIM25 knockout cells were constructed using the CRISPR-Cas9 gene-editing system. The CRISPR plasmid pEP-330x (Addgene) contains expression cassettes of Cas9 and puroMycin resistant gene. The target sequences of guide RNAs (gRNAs) were designed using the Massachusetts Institute of Technology online tool (http://crispr.mit.edu/) and synthesized from TSINGKE. Two gRNAs targeting the exons of TRIM25 were designed and inserted into the pEP-330x vector by using the Bpi I (Thermo Scientific) site and cotransfected into cells. After 48 hours, puroMycin (Sigma-Aldrich) was used for selection in HEK293 (2 μg $ml^{-1}$) and L929 (8 μg $ml^{-1}$). To validate and pick out the knockout cell colonies, genomic DNA was extracted from the parental and knockout cells and validated at the DNA level by PCR. Primers for constructing CRISPR-Cas9 plasmids and genotype identification are listed in table S3.

### Reporter assays

HEK293 cells ($2 \times 10^5$ cells $ml^{-1}$) were seeded on 96-well plates and transfected in triplicate with test plasmids and 90 ng of firefly luciferase reporter plasmids (pGL4.2-Luc) and 10 ng of *Renilla* luciferase reporter plasmids [pRL-TK (HSV-thymidine kinase promoter)] per well using polyethylenimine on the following day. An empty control plasmid was added to ensure that each transfection received the same amount of total DNA. Twenty-four hours after transfection, luciferase assays were performed using a dual-specific luciferase assay kit (Promega). Firefly luciferase activities were normalized on the basis of *Renilla* luciferase activities.

### ChIP–quantitative PCR assay

ChIP assays were performed according to the manufacturer's instructions with an EZ-Magna ChIP A/G kit (Millipore). Briefly, the Thp1 cells were fixed by 1% formaldehyde. The cross-linked chromatin was sonicated in a water bath at 4°C using Bioruptor UCD-200 sonicator to obtain DNA fragments sized between 100 and 500 base pairs. Chromatin from $1 \times 10^6$ Thp1 cells was used for each ChIP experiment. Antibodies against H3K4me3 (Millipore) and H3K27me3 (Millipore) were used. The DNA from cross-linking reversion was purified for quantitative PCR, using the following primers: 5′-GCTTTCCCAAAGGCCAGTTT-3′ (forward) and 5′-TTGTGCAGAAGAGCACTCCC-3′ (reverse).

### Lung histology

Lungs from control or virus-infected mice were dissected, fixed in 4% paraformaldehyde, embedded into paraffin, sectioned, stained with hematoxylin and eosin solution, and examined by light microscopy for histological changes.

### Human peripheral blood samples

A total of 77 peripheral blood samples were collected from children with bronchiolitis hospitalized in the Children's Hospital, Zhejiang University School of Medicine, and 40 age- and sex-matched healthy children were treated as a control group. Peripheral blood samples were obtained from the patients on admission. The detailed patient's information was described. This study was approved by the ethics committee of the Children's Hospital, Zhejiang University School of Medicine and was in compliance with institutional guidelines (no. 2018-016). Written informed consent was obtained from at least one guardian of each patient before enrollment. The detailed patient's information was shown in our previous study (*16*).

### Statistical analysis

Statistical analysis was performed with Prism v5.0 (GraphPad Software). For in vivo experiments, values were expressed as the means ± SD of $n$ animals, and data shown were representative of three independent experiments. Mouse survival curves and statistics were analyzed with the Mantel-Cox test. The level of statistically significant difference was defined as $P < 0.05$. No data points or mice were excluded from the study. No randomization or blinding was used.

## SUPPLEMENTARY MATERIALS

Supplementary material for this article is available at http://advances.sciencemag.org/cgi/content/full/5/2/eaav0163/DC1

Fig. S1. NDR2 specifically enhances RNA virus–induced IFN-β, IL-6, and TNF-α production in macrophages in a kinase-independent manner.
Fig. S2. NDR2 protects mice from RNA virus infections.
Fig. S3. NDR2 enhances RIG-I pathway activation in a kinase-independent manner.
Fig. S4. Schematic structure of NDR2 and TRIM25 and their derivatives.
Fig. S5. NDR2 promotes TRIM25-mediated K63-linked polyubiquitination of RIG-I.
Fig. S6. Virus infections inhibit NDR2 expression via STAT1-dependent mechanism.
Table S1. List of antibody information.
Table S2. List of primers for qPCR.
Table S3. List of gRNAs for CRISPR-CAS9.

## REFERENCES AND NOTES

1. O. Takeuchi, S. Akira, Pattern recognition receptors and inflammation. *Cell* **140**, 805–820 (2010).
2. Y. M. Loo, M. Gale Jr., Immune signaling by RIG-I-like receptors. *Immunity* **34**, 680–692 (2011).
3. K. Honda, A. Takaoka, T. Taniguchi, Type I interferon [corrected] gene induction by the interferon regulatory factor family of transcription factors. *Immunity* **25**, 349–360 (2006).
4. W. M. Schneider, M. D. Chevillotte, C. M. Rice, Interferon-stimulated genes: A complex web of host defenses. *Annu. Rev. Immunol.* **32**, 513–545 (2014).
5. M. U. Gack, Y. C. Shin, C.-H. Joo, T. Urano, C. Liang, L. J. Sun, O. Takeuchi, S. Akira, Z. Chen, S. Inoue, J. U. Jung, TRIM25 RING-finger E3 ubiquitin ligase is essential for RIG-I-mediated antiviral activity. *Nature* **446**, 916–920 (2007).
6. D. Gao, Y.-K. Yang, R.-P. Wang, X. Zhou, F.-C. Diao, M.-D. Li, Z.-H. Zhai, Z.-F. Jiang, D.-Y. Chen, REUL is a novel E3 ubiquitin ligase and stimulator of retinoic-acid-inducible gene-I. *PLOS ONE* **4**, e5760 (2009).
7. J. Yan, Q. Li, A. P. Mao, M. M. Hu, H. B. Shu, TRIM4 modulates type I interferon induction and cellular antiviral response by targeting RIG-I for K63-linked ubiquitination. *J. Mol. Cell Biol.* **6**, 154–163 (2014).
8. K. Kuniyoshi, O. Takeuchi, S. Pandey, T. Satoh, H. Iwasaki, S. Akira, T. Kawai, Pivotal role of RNA-binding E3 ubiquitin ligase MEX3C in RIG-I-mediated antiviral innate immunity. *Proc. Natl. Acad. Sci. U.S.A.* **111**, 5646–5651 (2014).
9. K. Arimoto, H. Takahashi, T. Hishiki, H. Konishi, T. Fujita, K. Shimotohno, Negative regulation of the RIG-I signaling by the ubiquitin ligase RNF125. *Proc. Natl. Acad. Sci. U.S.A.* **104**, 7500–7505 (2007).

10. W. Chen, C. Han, B. Xie, X. Hu, Q. Yu, L. Shi, Q. Wang, D. Li, J. Wang, P. Zheng, Y. Liu, X. Cao, Induction of Siglec-G by RNA viruses inhibits the innate immune response by promoting RIG-I degradation. *Cell* **152**, 467–478 (2013).
11. W. Liu, J. Li, W. Zheng, Y. Shang, Z. Zhao, S. Wang, Y. Bi, S. Zhang, C. Xu, Z. Duan, L. Zhang, Y. L. Wang, Z. Jiang, W. Liu, L. Sun, Cyclophilin A-regulated ubiquitination is critical for RIG-I-mediated antiviral immune responses. *eLife* **6**, e24425 (2017).
12. A. Hergovich, M. R. Stegert, D. Schmitz, B. A. Hemmings, NDR kinases regulate essential cell processes from yeast to humans. *Nat. Rev. Mol. Cell Biol.* **7**, 253–264 (2006).
13. H. Cornils, R. S. Kohler, A. Hergovich, B. A. Hemmings, Downstream of human NDR kinases: Impacting on c-Myc and p21 protein stability to control cell cycle progression. *Cell Cycle* **10**, 1897–1904 (2011).
14. A. Vichalkovski, E. Gresko, H. Cornils, A. Hergovich, D. Schmitz, B. A. Hemmings, NDR kinase is activated by RASSF1A/MST1 in response to Fas receptor stimulation and promotes apoptosis. *Curr. Biol.* **18**, 1889–1895 (2008).
15. E. Devroe, P. A. Silver, A. Engelman, HIV-1 incorporates and proteolytically processes human NDR1 and NDR2 serine-threonine kinases. *Virology* **331**, 181–189 (2005).
16. Z. Liu, Q. Qin, C. Wu, H. Li, J. Shou, Y. Yang, M. Gu, C. Ma, W. Lin, Y. Zou, Y. Zhang, F. Ma, J. Sun, X. Wang, Downregulated NDR1 protein kinase inhibits innate immune response by initiating an miR146a-STAT1 feedback loop. *Nat. Commun.* **9**, 2789 (2018).
17. H. Cornils, M. R. Stegert, A. Hergovich, D. Hynx, D. Schmitz, S. Dirnhofer, B. A. Hemmings, Ablation of the kinase NDR1 predisposes mice to the development of T cell lymphoma. *Sci. Signal.* **3**, ra47 (2010).
18. A. Suzuki, T. Ogura, H. Esumi, NDR2 acts as the upstream kinase of ARK5 during insulin-like growth factor-1 signaling. *J. Biol. Chem.* **281**, 13915–13921 (2006).
19. S. Chiba, Y. Amagai, Y. Homma, M. Fukuda, K. Mizuno, NDR2-mediated Rabin8 phosphorylation is crucial for ciliogenesis by switching binding specificity from phosphatidylserine to Sec15. *EMBO J.* **32**, 874–885 (2013).
20. K. Rehberg, S. Kliche, D. A. Madencioglu, M. Thiere, B. Muller, B. M. Meineke, C. Freund, E. Budinger, O. Stork, The serine/threonine kinase Ndr2 controls integrin trafficking and integrin-dependent neurite growth. *J. Neurosci.* **34**, 5342–5354 (2014).
21. M. R. Stegert, R. Tamaskovic, S. J. Bichsel, A. Hergovich, B. A. Hemmings, Regulation of NDR2 protein kinase by multi-site phosphorylation and the S100B calcium-binding protein. *J. Biol. Chem.* **279**, 23806–23812 (2004).
22. S. Bhattacharya, E. Large, C. W. Heizmann, B. A. Hemmings, W. J. Chazin, Structure of the $Ca^{2+}$/S100B/NDR kinase peptide complex: Insights into S100 target specificity and activation of the kinase. *Biochemistry* **42**, 14416–14426 (2003).
23. G. Meroni, G. Diez-Roux, TRIM/RBCC, a novel class of 'single protein RING finger' E3 ubiquitin ligases. *Bioessays* **27**, 1147–1157 (2005).
24. M. Rentoft, K. Kim, Y. Cho, C. H. Lee, A. Kim, Enhancer requirement for histone methylation linked with gene activation. *FEBS J.* **275**, 5994–6001 (2008).
25. E. Devroe, H. Erdjument-Bromage, P. Tempst, P. A. Silver, Human Mob proteins regulate the NDR1 and NDR2 serine-threonine kinases. *J. Biol. Chem.* **279**, 24444–24451 (2004).
26. T. Millward, P. Cron, B. A. Hemmings, Molecular cloning and characterization of a conserved nuclear serine(threonine) protein kinase. *Proc. Natl. Acad. Sci. U.S.A.* **92**, 5022–5026 (1995).
27. M. Gu, Z. Liu, R. Lai, S. Liu, W. Lin, C. Ouyang, S. Ye, H. Huang, X. Wang, RKIP and TBK1 form a positive feedback loop to promote type I interferon production in innate immunity. *EMBO J.* **35**, 2553–2565 (2016).
28. L. Hu, J. Xu, X. Xie, Y. Zhou, P. Tao, H. Li, X. Han, C. Wang, J. Liu, P. Xu, D. Neculai, Z. Xia, Oligomerization-primed coiled-coil domain interaction with Ubc13 confers processivity to TRAF6 ubiquitin ligase activity. *Nat. Commun.* **8**, 814 (2017).

**Acknowledgments**
**Funding:** This work was supported by grants from the National Basic Research Program of China (973) (2014CB542101), the National Natural Science Foundation of China (31770932 and 31570864), and the National Postdoctoral Science Foundation of China (2018M632485 and 2018T110605). **Author contributions:** X.W. designed the research. Z.L., C.W., Y.P., H.L., X.M.W., Y.Y., M.G., and Y.Z. performed research. X.W. and Z.L. analyzed data and wrote the paper. **Competing interests:** The authors declare that they have no competing interests. **Data and materials availability:** All data needed to evaluate the conclusions in the paper are present in the paper and/or the Supplementary Materials. Additional data related to this paper may be requested from the authors.

Submitted 6 August 2018
Accepted 20 December 2018
Published 6 February 2019
10.1126/sciadv.aav0163

**Citation:** Z. Liu, C. Wu, Y. Pan, H. Liu, X. Wang, Y. Yang, M. Gu, Y. Zhang, X. Wang, NDR2 promotes the antiviral immune response via facilitating TRIM25-mediated RIG-I activation in macrophages. *Sci. Adv.* **5**, eaav0163 (2019).